Distributed Diameter Subcoil Twisted Loop Antenna in Nonradiative WPT

Marjorie Grzeskowiak, Antoine Diet, Megdouda Benamara, Patrick Poulichet, Christophe Conessa, Stéphane Protat, Marc Biancheri-Astier, Francisco de Oliveira Alves, Yann Le Bihan, Gaelle Bazin Lissorgues

Distributed Diameter Subcoil Twisted Loop Antenna in Nonradiative WPT

Marjorie Grzeskowiak, Antoine Diet, Megdouda Benamara, Patrick Poulichet, Christophe Conessa, Stéphane Protat, Marc Biancheri-Astier, Francisco de Oliveira Alves, Yann Le Bihan, and Gaelle Lissorgues

***Abstract*—This letter focuses on the high-frequency wireless power transfer by electromagnetic induction and its dependence on the lateral misalignment and tilt of the small receiving coil relative to the transmitting coil. We combine two structures, the twisted loop antenna (TLA) and subcoils of a distributed diameter coil (DDC) for transmitting designs. Our system is then referred to as TLA-DDC. The radius of the subcoils is parametrically varied for different distances between the coils and performed in two positions for each distance (coaxial position when the receiving coil is parallel to the plane of the transmitting coil, and center position for the perpendicular orientation of both coils). Then, using different radii for the transmitting DDC TLA when the receiving coil is moved onto its surface allows us to obtain a greater value of efficiency at different positions: up to 2.4 times for the peak value and 1.5 for the average value for receiving coil in parallel plane. The efficiency of the magnetic coupling is determined by means of power efficiency with a comparison between the DDC TLA antennas and a standard coil antenna corresponding to the same inductance value.**

***Index Terms*—Current distribution, magnetic coupling, wireless power transfer (WPT).**

I. Introduction

In 13.56 MHz radio frequency identification (RFID) or in inductive wireless power transfer (WPT), the active area depends on the intensity and orientation of the magnetic field generated by the transmitting coils [1]. With the growing trend towards miniaturization of receiving coils, it is a difficult challenge to design a planar transmitting coil that powers the receiving coil circuit at the required read-out distance, whatever its orientation, over a large area or in a large volume [2], [3].

The twisted loop antenna (TLA) [4], constituted of two complementary loops, whose current drives in opposite orientation, allows the electromagnetic induction to be less affected by the relative tilting direction of the transmitting coil versus the receiving one. The distributed diameter coil (DDC) [5], constituted of a combination of turns of multiple diameters, reduces the degradation of the electromagnetic induction by the relative location of the transmitting coil to the receiving coil. The combination of the TLA and the DDC in transmitting design can improve the link efficiency whatever the lateral and angular misalignment.

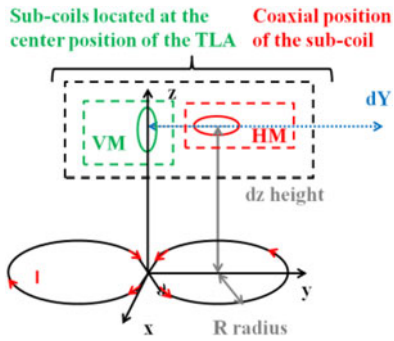

Fig. 1. Studied DDC TLA transmitting and receiving system.

In Section II, the radius of the transmitting TLA is studied for different distances between the coils in order to optimize the coupling coefficient. The displacement of the receiving coil onto the surface of the transmitting coil shows a greater value of coupling coefficient in combining three radii at a fixed distance. The number of the subcoils is varied in Section III while keeping constant the inductance, and the studied transmitting TLA is presented. Section IV compares by electromagnetic simulation the performances of the transmitting coils with a receiving coil, whose effective area is less than 1/40 of the transmitting coil. To conclude, the optimized structures are fabricated, and the measured results of power efficiency are compared to the simulated ones.

II. Optimization of DDC Radii

A. Coaxial Coils

Fig. 1 shows that the TLA is constituted of two circles connected with a cross connection of conductors at the center. The radius R of the TLA subcoils is increased, and the coupling coefficient between the transmitting and receiving coils is carried out using the magneto-statics module Radia [6]. This is done for both configurations of the receiving coil: in horizontal mode (HM) when the receiving coil and subcoils are in ($x0y$) plane and placed coaxially, and in vertical mode (VM) when the receiving coil is oriented perpendicularly in the center of the TLA structure in ($x0z$) plane.

Obviously, the level of the coupling coefficient decreases as the distance increases between the coaxial coils in HM and VM modes [see Fig. 2 (a) and (b)] [1]. However, maximum of

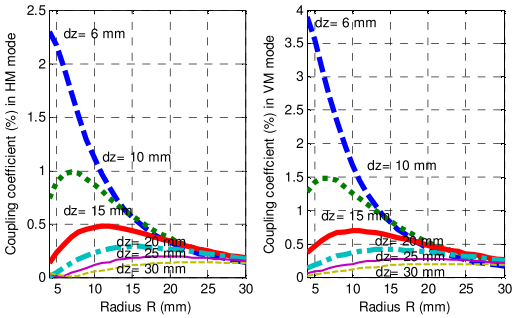

Fig. 2. Simulated coupling coefficient *k* (%) versus the radius *R* of the transmitting coil at distance *dz* in HM and in VM modes using Radia.

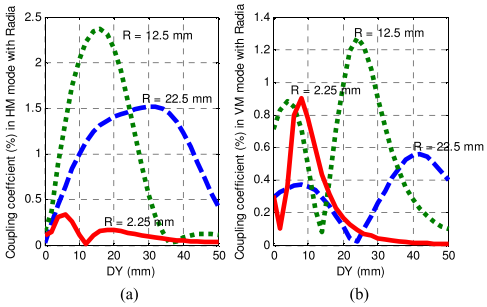

Fig. 3. Simulated coupling coefficient *k* (%) versus the DY misalignment at 10 mm height for radii *R* (2.25 mm; 12.5 mm; 22.5 mm) (a) HM and (b) VM modes using Radia.

coupling coefficient depends on the radius of the transmitting coil. As shown in Fig. 2, subcoils of different radii should be used to maximize the inductive coupling for different distances in HM and VM modes.

B. Misaligned Coils

In order to observe the magnetic coupling onto the surface of the transmitting TLA, the receiving coil is moved from the center position to the edge of the transmitting coil (loop), at an arbitrary height of 10 mm. Three radii of the transmitting coil are 2.25, 12.5, and 22.5 mm.

In HM mode [see Fig. 3 (a)], the coils with 12.5 and 22.5 mm radius seem efficient and complementary over different zones. In HM mode, corresponding to the receiving coil in (*x0y*) plane as shown in Fig. 1, the inductive coupling depends on the integration of the *Z*-component of *B*-field, and is maximum in the center of the subcoils. In VM mode, corresponding to the receiving coil in (*x0z*) plane (see Fig. 1), the coupling coefficient calculated by the integration of *y*-component is disrupted by the *X*-component on Fig. 4. Although, due to anti-symmetric (*xOz*) plane, *Bx* should be null on the (*y*)-axis, and especially in the center of the structure, while it is not the case on the Fig. 4.

To explain the origin of *Bx* component, the magnetic induction is calculated on Fig. 5 without the connection between the complementary subcoils while keeping the current flow direction as previously (see Fig. 1): *Bx* is null. Furthermore, in presence of the receiving coil, the *Y*-component is completely modified: The value is superior above the exterior edge of the structure.

The disturbance of the crossed connection could reduce the inductive coupling in VM mode. Another degree of freedom can be added in varying the current for each radius of the subcoil structure and the position of the subcoils inside the TLA area.

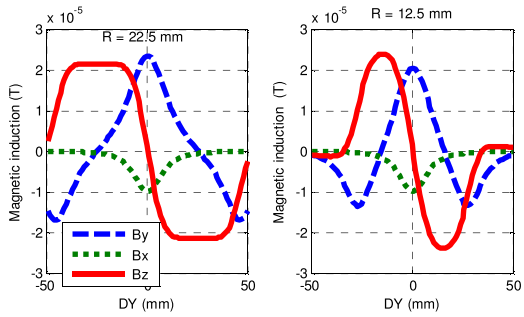

Fig. 4. Simulated magnetic induction versus DY misalignment at 10 mm for radii *R* of 22.5 and 12.5 mm with cross connection and without receiving coils.

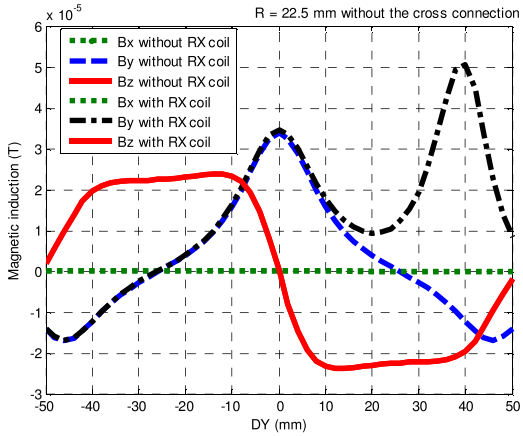

Fig. 5. Simulated magnetic induction versus DY misalignment at 10 mm for radius *R* of 22.5 mm with and without the receiving coil and without the cross connection.

III. Optimization and Design of DDC Turns

Each receiving subcoil can be coaxially (on-center) or non-coaxially (off-center) placed inside the loops of the TLA. The enameled copper wire is rolled in the slots of the fabricated plastic base. In the case of the coaxial subcoils, the sum L_1 of the self-inductances of half of the transmitting coil [7] can be calculated without consideration of mutual inductance between each subcoil by

$$L_{d_i}^{N_i} = 2\pi d_i ln\left(\frac{\pi d_i}{d_w}\right) N_i^{1.9} \quad L_1 = L_{d_1}^{N_1} + L_{d_2}^{N_2} + L_{d_3}^{N_3} \quad (1)$$

where d_i and N_i correspond to the diameter and the number of turns of the subcoils, respectively, d_w to the wire diameter. The mutual inductance $M_{a,b}$ between each coaxial subcoil can be calculated by (2) as given in [5]

$$M_{a,b} = N_a N_b \mu_0 \sqrt{ab}\left[\left(\frac{2}{\kappa} - \kappa\right) K(\kappa) - \frac{2}{\kappa} E(\kappa)\right] \quad (2)$$

where

$$\kappa = \left(\frac{4ab}{(a+b)^2}\right)^{1/2} \quad (3)$$

and a and b are the radii of the coaxial subcoils, $K(\kappa)$ and $E(\kappa)$ are the complete elliptic integrals of the first and second kind, respectively, and N_a and N_b are the turn numbers of the considered subcoils diameter. The values of self-inductances have been performed using MATLAB [8] and are composed between L_{DDCmin} and L_{DDCmax} when considering the

TABLE I
CALCULATED, SIMULATED, AND MEASURED INDUCTANCE OF THE DISTRIBUTED DIAMETER SUBCOILS TWISTED LOOP ANTENNA

	Conventional		On-Center		Off-Center		
N_1, N_2, N_3	300	400	230	137	220	240	320
L_{DDCmin} (μH)	2.07	3.31	2.13	1.67	2.03	4.1	3.58
L_{DDCmax} (μH)	2.19	3.52	2.25	1.78			
Simulated L_{DDC} (μH)	1.94	3.27	1.98	1.77	1.64	3.27	3.05
Measured L_{DDC} (μH)	2.38	Ø	2.79	2.26	2.17	Ø	Ø
Simulated R_{DDC} (Ω)	2.2	3.17	2.2	3.4	1.71	2.81	2.5
Measured R_{DDC} (Ω)	3.1	Ø	4.4	3.4	2.2	Ø	Ø

manufacturer data: wire diameter between 0.012 and 0.021 cm. The commonly known mathematical formulas, from the integral of small current portion in the wire, have been modified and generalized in [9] to be applicable for calculation of the mutual inductance of thin noncoaxial coils with parallel axes. Without analytical formulas for noncoaxial coils, Radia is used to calculate the inductance of the DDC coils. HFSS [10] is performed to determine the simulated inductance of the DDC coils when each subcoil is connected.

The reference name associated to an inductance of Table I is defined with three numbers that represent the number of turns of each external radii r_1, r_2, and r_3 (respectively 22.5, 12.5, and 2.25 mm). For instance, the conventional TLA is 300 (three turns of r_1, $0\,r_2$, $0\,r_3$). The simulated values can reach a maximum of 7.3% discrepancy with the empirical ones. In Table I, the discrepancies between the measured values (measured L_{DDC}) extracted by Rhode & Schwarz ZnB8 vector network analyzer and the simulated one (simulated L_{DDC}) can be provided by the 20 cm twisted enameled wire to connect the coils with the SMA connector: 55 cm length of wire corresponds to 48 pF capacitance that increases the values of measured inductance.

The comparison in terms of coupling with small receiving coil is studied in Section IV for each structure.

IV. SIMULATED POWER EFFICIENCY

To quantify the magnetic coupling, the power efficiency η is used: It depends on the mutual inductance M and on the electrical characteristics of the coil

$$\eta = \frac{(\omega M)^2}{(R_L + Z_{22})\left((Z_{11})(R_L + Z_{22}) + (\omega M)^2\right)}. \quad (4)$$

The impedance parameters are

$$Z_{11} = \left(R_1 + \frac{1}{jC_1\omega}\right) + jL_1\omega \quad (5)$$

$$Z_{12} = jM\omega \; = Z_{21}$$

$$Z_{22} = \left(R_2 + \frac{1}{jC_2\omega}\right) + jL_2\omega.$$

The inductances for TX DDC TLA and RX coils are, respectively, L_1 ($= L_{\mathrm{DDC}}$ in Table I) and L_2 ($= 0.031$ μH); the resistances are equal to R_1 ($= R_{\mathrm{DDC}}$ in Table I) and R_2 (0.31 Ω). The receiving coil is loaded by 50 Ω resistance (R_L). The transmitting and receiving coils are tuned, respectively, with C_1 and C_2 capacitors.

The power efficiency is calculated for the structures in Table I and reported versus the simulated self-inductance. Fig. 7 shows the maximum simulated power efficiency versus the inductances

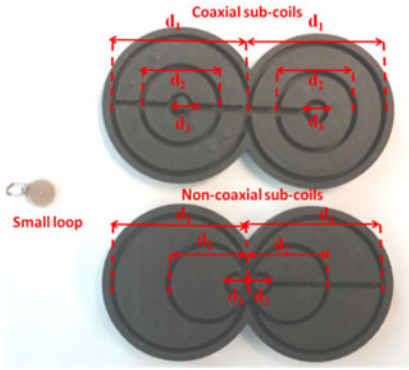

Fig. 6. Three-dimensional fabricated plastic bases ($d_1 = 4.5$ cm, $d_2 = 2.5$ cm, $d_3 = 0.45$ cm) with a small receiving coil (left).

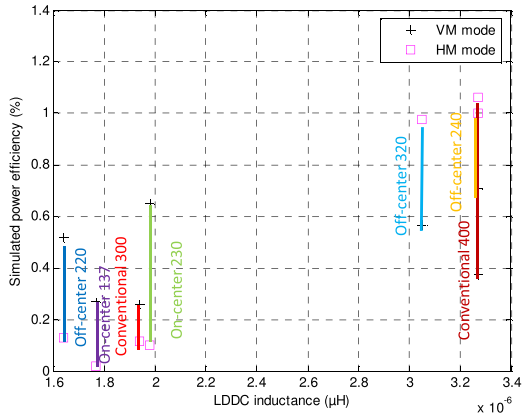

Fig. 7. Simulated maximum power efficiency versus the L_{DDC} inductance.

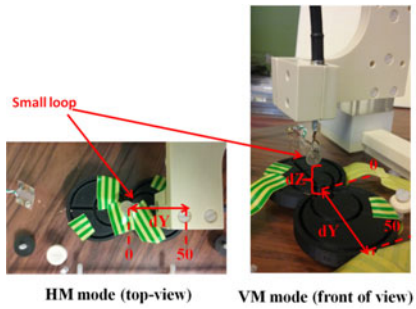

Fig. 8. Experimental setup in HM mode and VM mode.

of the transmitting coil for both VM and HM modes at 10 cm. Two parts appear: one that favors the HM mode with a DDC inductance around 2 μH, and the other one around 3.2 μH improving the VM mode.

The performance of the on-center (230 and 137) in comparison with the 300 conventional coil has been done with HFSS simulation and was validated by HF RFID detection [11]. We measured the greatest RFID read-out distance at one point for two tag diameters: As seen on B-field displays in [11], the effective area of the on-center structure improves the tag detection for a tag with similar diameter.

V. EXPERIMENTAL MEASUREMENT SETUP

The experimental setup allows us to vary DY misalignment and *dz* height in HM mode [see Fig. 8(a)] and in VM mode [see Fig. 8(b)].

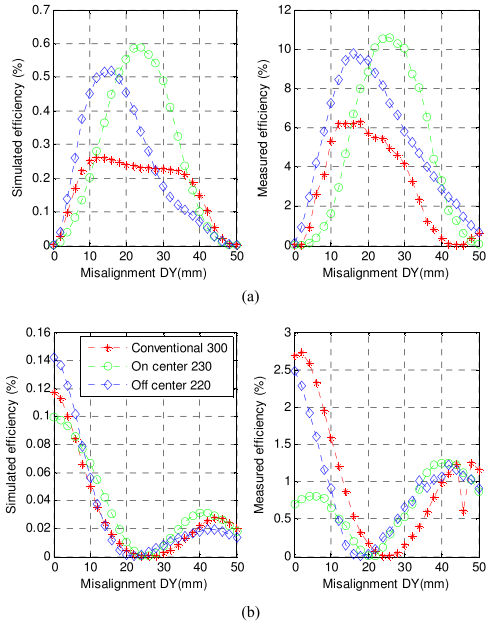

Fig. 9. Simulated and measured efficiency (%) versus the misalignment DY. (a) In HM mode. (b) In VM mode.

The power efficiency is reported versus misalignment DY for the conventional TLA, the on-center 230 and the off-center 220 in HM [see Fig. 9(a)] and in VM modes [see Fig. 9(b)]. The inductance of TX coil is reported in Table I. The RX spiral small coil is made by microetching (strip of 110 μm, inter-spire of 110 μm, and 21 turns inside 1 cm diameter) on both sides of the FR4 substrate. The measurement of resistance and inductance gave, respectively, 10 Ω and 3.6 μH. The TX and RX coils are tuned with external capacitors. In Fig. 9, the simulated and measured efficiencies deviate in terms of amplitude. The level is different because the receiving coil is 1-turn coil in simulation despite it corresponding to 21-turns coil. The simulation of 21-turns received coil is not possible with HFSS because of number of meshing cells: The size of the received coil, especially the width of slots and strip lines, is small in comparison with the working wavelength to calculate efficiency from the impedance matrix. In order to simplify the structure, if we calculate the efficiency for each radius of 1-turn coil, the coupling between each loop of the 21-turn coil would be neglected. In order to obtain the simulated efficiency, we calculate the average received area for the 21-turn coil, which corresponds to a ratio of 15 between the 21-turn coil and the 1-turn coil of 10 mm diameter and to the discrepancy between finite element method simulation and measurement. In HM mode, the DDC TLA structures improve the maximum value of the efficiency in keeping almost constant the area where the coupling is efficient with the conventional coil.

In tilt scenarios with the newly designed coil, the simulated efficiency for the off-center 220 should be better in comparison with the conventional TLA: The 220 off-center that is slightly weaker than the conventional coil in VM mode, and better in HM mode, seems more robust due to less wires in cross connection. When the receiving coil is rotated, the peak level decreased from the value in HM mode to the one in VM mode, while the position where it appears varies from center to edge of the subcoil (see Fig. 10).

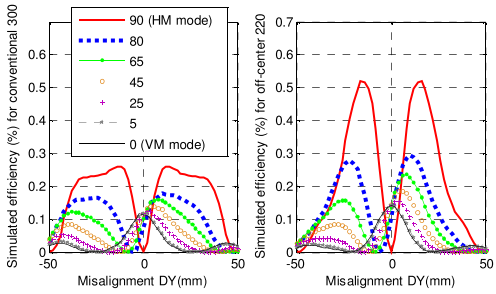

Fig. 10. Simulated efficiency (%) versus (y) misalignment for rotation angle of receiving coil.

To minimize the disturbance of the cross connection, squared coils would be preferred in future work with connection realized by wires in reverse current [12].

VI. Conclusion

DDC TLA subcoils applied to WPT systems offer several possibilities of modifying the distribution and orientation of the magnetic field. This new design approach proposes an enhancement of the maximum inductive coupling with the receiving coil up to 149% in comparison with the conventional TLA, while achieving an average coupling over a larger area or volume. Magneto-static and magneto-dynamic softwares were used to optimize the coupling efficiency. It is expected that the proposed coil structure will be well applied to free positioning small WPT systems, placed on arbitrary oriented objects for instance on a movable tray.

References

[1] K. Finkenseller, *RFID Handbook: Radio-Frequency Identification Fundamentals and Application*, 2nd ed. New York, NY, USA: Wiley, 2003.

[2] B. H. Waters *et al.*, "Optimal coil size ratios for wireless power transfer applications," in *Proc. Int. Symp. IEEE Circuits Syst.*, Jun. 2014, pp. 2045–2048, doi: 10.1109/ISCAS.2014.6865567.

[3] X. Shi *et al.*, "Large area wireless power via a planar array of coupled resonators," in *Proc. Int. Workshop IEEE Antenna Technol.*, Mar. 2016, pp. 200–203, doi: 10.1109/IWAT.2016.7434842.

[4] M. Benamara *et al.*, "Twisted loop antenna for HF RFID detection surface," in *Proc. 10th Eur. Conf. IEEE Antennas Propag.*, Apr. 2016, doi: 10.1109/EuCAP.2016.7481810.

[5] A. Diet *et al.*, "Improvement of RFID HF tags detection with a distributed diameter coil," *IEEE Antennas Wireless Propag. Lett.*, vol. 15, pp. 1943–1946, 2016, doi: 10.1109/LAWP.2016.2544540.

[6] Radia, ver. 4.1. [Online]. Available: http://www.esrf.eu/Accelerators/Groups/InsertionDevices/Software/Radia

[7] C. M. Zierhofer *et al.*, "Geometric approach for coupling enhancement of magnetically coupled coils," *IEEE. Trans. Biomed. Eng.*, vol. 43, no.7, pp. 708–714, Jul. 1996, doi: 10.1109/10.503178.

[8] MATLAB, ver. 7. [Online]. Available: http://fr.mathworks.com/products/matlab/

[9] V. Pankrac, "Generalization of relations for calculating the mutual inductance of coaxial coils in terms of their applicability to non-coaxial coils," *IEEE. Trans. Magn.*, vol. 47, no. 11, pp. 4554–4563, Nov. 2011, doi: 10.1109/TMAG.2011.2148175.

[10] Ansys HFSS, ver. 14. [Online]. Available: http://www.ansys.com/Products/Simulation+Technology/Electronics/Signal+Integrity/ANSYS+HFSS

[11] M. Grzeskowiak *et al.*, "Coaxially distributed diameter sub-coil twisted loop antenna in HF RFID," in *Proc. 10th Eur. Conf. IEEE Antennas Propag.*, Mar. 2017, doi: 10.23919/EuCAP.2017.7928426.

[12] A. Diet *et al.*, "LF RFID chequered loop antenna for pebbles on the beach detection," in *Proc. 46th Eur. Conf. IEEE Microw.*, Oct. 2016, doi: 10.1109/EuMC.2016.7824272.